


Searching strong ‘spin’-orbit coupled one-dimensional hole gas in strong magnetic fields

Rui Li (李睿) ^{1,*}

¹*Key Laboratory for Microstructural Material Physics of Hebei Province,
School of Science, Yanshan University, Qinhuangdao 066004, China*

(Dated: July 5, 2021)

We show that a strong ‘spin’-orbit coupled one-dimensional (1D) hole gas is achievable via applying a strong magnetic field to the originally two-fold degenerate hole gas confined in a cylindrical Ge nanowire. Both strong longitudinal and strong transverse magnetic fields are feasible to achieve this goal. The induced low-energy subband dispersion of the hole gas can be written as $E = \hbar^2 k_z^2 / (2m_h^*) + \alpha \sigma^z k_z + g_h^* \mu_B B \sigma^x / 2$, a form that is exact the same as that of the electron gas in the conduction band. Also, the induced hole effective m_h^* ($0.07 \sim 0.08 m_e$) and the ‘spin’-orbit coupling α ($0.4 \sim 0.65$ eV Å) have a small magnetic field dependence, while the effective g -factor g_h^* of the hole ‘spin’ only has a small magnetic field dependence in the large fields region.

I. INTRODUCTION

There are well developed techniques for initialization, manipulation, and readout of the electron spin states in gate-defined semiconductor quantum dots [1, 2], such that the quantum dot electron spin has been regarded as one of the most promising qubit candidates for implementing quantum computations [3]. Owing to a suppressed interaction between the hole spin and the lattice nuclear spins, quantum dot hole spin is also expected to be an excellent qubit candidate as well as the electron spin [4]. Meanwhile, the band dispersions near the top of the valence band of semiconductors are described by the Luttinger-Kohn Hamiltonian [5, 6], where there is a large intrinsic spin-orbit coupling, such that the quantum dot hole spin has a merit of being manipulable by an external oscillating electric field [7, 8].

Planar (2D) [9, 10] or nanowire (1D) [11–15] hole quantum dot can be fabricated experimentally via placing proper metallic gates below a 2D or 1D hole gas. Note that the physics of the hole spin qubit in a planar quantum dot may be totally different from that in a nanowire quantum dot. Take the recently extensively studied semiconductor Ge as an illustration [16–21], the lowest subband dispersion of the 2D hole gas in a Ge quantum well always has heavy hole character [22], and can be modeled by a parabolic curve with band minimum at the center of the k space [23]. While the low-energy subband dispersions of the 1D hole gas in a cylindrical Ge nanowire are quite different [24]. The lowest two subband dispersions of the 1D hole gas anticross with each other at the center of the k_z space [24, 25], and the shape of the dispersion is very similar to that of a strong spin-orbit coupled 1D electron gas described by the Hamiltonian $H_c = p^2 / (2m_e^*) + \alpha \sigma^z p + g_e \mu_B B \sigma^x / 2$ [26, 27]. However, there is an additional spin degeneracy in the hole subband dispersions [25]. We note that the above strong

spin-orbit coupled electron gas model has many applications in the studies of the spin-orbit qubits [28–35], the Bose-Einstein condensations [36–38], and the Majorana fermions [39, 40].

In this paper, we are inspired to achieve a strong spin-orbit coupled 1D hole gas in a cylindrical Ge nanowire, which would share similar potential applications with the electron gas. In order to achieve a pure (without the hole spin degeneracy) ‘spin’-orbit coupled 1D hole gas, we apply a strong magnetic field to split off the unwanted spin degree of freedom in the hole subband dispersions. Note that the ‘spin’ here is more properly regarded as a pseudo spin, it is introduced to describe the induced low-energy subband dispersion of the hole gas in a strong magnetic field in comparison with the conduction band electron case. Because both the longitudinal and the transverse g -factors of the hole gas at the band minimum are finite and are comparable to each other [25], such that both strong longitudinal and strong transverse magnetic fields are feasible to achieve this splitting goal. The form of the induced low-energy hole subband dispersion is completely the same as that of the conduction band electron case, i.e., described by $E = \hbar^2 k_z^2 / (2m_h^*) + \alpha \sigma^z k_z + g_h^* \mu_B B \sigma^x / 2$. The magnetic field dependences of the hole effective mass m_h^* , the strength of ‘spin’-orbit coupling α , and the effective g -factor g_h^* (for the pseudo hole spin) are discussed in details.

II. 1D HOLE GAS

We are interested in a 1D hole gas, which is confined in a cylindrical Ge nanowire of radius R . The axis direction of the nanowire is defined as the z -direction. For semiconductor Ge in the bulk, the band dispersions near the top of the valence band are well described by the Luttinger-Kohn Hamiltonian in the spherical approximation [6, 41]. Hence, using the language of the effective mass approximation, we write the Hamiltonian of a hole confined in

* rui.li@ysu.edu.cn

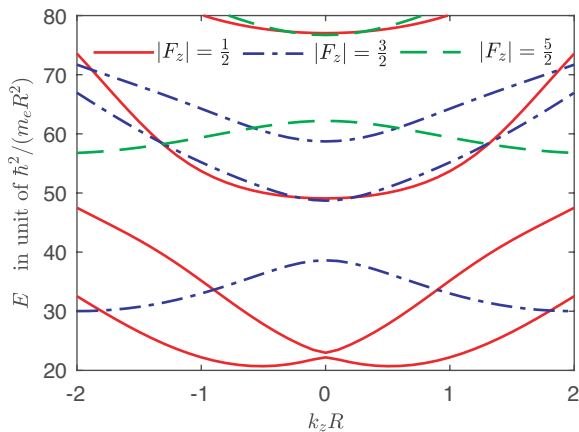


FIG. 1. The low-energy subband dispersions of the 1D hole gas. For a cylindrical Ge nanowire with radius $R = 10$ nm, the energy unit is $\hbar^2/(m_e R^2) \approx 0.763$ meV.

this nanowire as [24, 42, 43]

$$H_0 = \frac{1}{2m_e} \left[\left(\gamma_1 + \frac{5}{2}\gamma_s \right) \mathbf{p}^2 - 2\gamma_s (\mathbf{p} \cdot \mathbf{J})^2 \right] + V(r), \quad (1)$$

where m_e is the bare electron mass, $\gamma_1 = 13.35$ and $\gamma_s = (2\gamma_2 + 3\gamma_3)/5 = 5.11$ are Luttinger parameters [44] for semiconductor Ge, $\mathbf{p} = -i\hbar\nabla$ is the momentum operator, $\mathbf{J} = (J_x, J_y, J_z)$ is a spin-3/2 vector operator, and $V(r)$ is the transverse (xy plane) confining potential of the hole

$$V(r) = \begin{cases} 0, & r < R, \\ \infty, & r > R, \end{cases} \quad (2)$$

with R being the radius of the Ge nanowire. It should be noted that in our following calculations, we have chosen a representative and experimentally achievable nanowire radius $R = 10$ nm [11, 12].

The model (1) is exactly solvable, the detailed description of the solving method can be found elsewhere [25, 45, 46]. The z -component of the total angular momentum $F_z = -i\partial_\varphi + J_z$ is a conserved quantity $[F_z, H_0] = 0$, such that we can classify the eigenfunctions of H_0 using F_z [25, 46]. Following the method introduced in Ref. [45, 46], we obtain the low-energy subband dispersions of the 1D hole gas, which are explicitly shown in Fig. 1. As one can see clearly from the figure, the band minimum is not at the center of the k_z space. Instead, there are two symmetrical minimums approximately located at $|k_z R| \approx 0.517$. Also, for wave vectors in the interval $|k_z R| < 1$, the lowest two subband dispersions, i.e., given by total angular momentum $|F_z| = 1/2$ (see Fig. 1), are approximately separated from the other higher subband dispersions.

The shape of the lowest two subband dispersions of the hole gas shown in Fig. 1 is very similar to that of a strong spin-orbit coupled 1D electron gas, e.g., described by the Hamiltonian $H_c = p^2/(2m_e^*) + \alpha\sigma^z p + g_e\mu_B B\sigma^x/2$ [26, 27]. However, there is a spin degeneracy in the hole subband dispersions [25], while there is

no degeneracy for the electron case. Note that the spin degeneracy in the hole subband dispersions is a direct consequence of the coexistence of the time-reversal symmetry and the spin-rotation symmetry of the model (1). Here, we are motivated to search the strong ‘spin’-orbit coupled 1D hole gas via applying a strong magnetic field to lift out the unwanted spin degeneracy in the hole subband dispersions (see Fig. 1). As we have demonstrated in our previous paper [25], both the longitudinal and the transverse g -factors of the hole gas at the band minimum have finite values and are comparable to each other, such that both longitudinal and transverse magnetic fields are feasible to achieve this goal.

For a given energy eigenvalue $E_n(k_z)$ at a given wave vector k_z , we can obtain the corresponding eigenfunction via fixing the total angular momentum F_z , e.g., see Fig. 3 of Ref. [25]. Once one eigenfunction, e.g. $\Psi_{n,k_z,\uparrow}$ (n is the subband index), is obtained, the other degenerate counterpart, i.e., $\Psi_{n,k_z,\downarrow}$, can be obtained via a combination of the time-reversal and the spin-rotation transformations [25]. At a given wave vector k_z , we collect the lowest four eigenfunctions with total angular momentum $|F_z| = 1/2$, i.e., $\Psi_{1,k_z,\uparrow}$, $\Psi_{1,k_z,\downarrow}$, $\Psi_{2,k_z,\uparrow}$, and $\Psi_{2,k_z,\downarrow}$, which span the quasi-degenerate Hilbert subspace in our following perturbation calculations (see appendix A).

III. 1D HOLE GAS IN A STRONG LONGITUDINAL MAGNETIC FIELD

We now apply a strong longitudinal magnetic field $\mathbf{B} = (0, 0, B)$ to the 1D hole gas. In addition to adding a bare Zeeman term $2\kappa\mu_B B J_z$ to the hole Hamiltonian (1), we also need to make the following replacement on the momentum operator $\mathbf{p} \rightarrow \mathbf{p} + \mathbf{eA}$. Here $\kappa = 3.41$ is the Luttinger magnetic constant for semiconductor Ge [44] and $\mathbf{A} = (-By/2, Bx/2, 0)$ is the vector potential. We can rewrite the hole Hamiltonian as $H = H_0 + H^{(p)}$, where the zeroth order Hamiltonian H_0 is given by Eq. (1), and $H^{(p)}$ is the perturbation Hamiltonian consisting of both the bare Zeeman term and all the orbital terms of the magnetic field (for details see appendix B).

The presence of the magnetic field \mathbf{B} breaks the time-reversal symmetry of the hole Hamiltonian, such that the spin degeneracy in the hole subband dispersions (given in Fig. 1) is expected to be lifted by this field. Here, we focus only on the Hilbert subspace spanned by the lowest four subband wave-functions, i.e., $\Psi_{1,k_z,\uparrow}$, $\Psi_{1,k_z,\downarrow}$, $\Psi_{2,k_z,\uparrow}$, and $\Psi_{2,k_z,\downarrow}$. We use quasi-degenerate perturbation theory, i.e., the Hamiltonian $H = H_0 + H^{(p)}$ is written as a 4×4 matrix in this Hilbert subspace (for details see appendix B), to calculate the splittings among the lowest two subband dispersions. The results under various strong longitudinal magnetic fields are shown in Fig. 2. As we increase the magnetic field, there is an eye visible splitting in the originally two-fold degenerate subband dispersions. Now, the low-energy physics of the

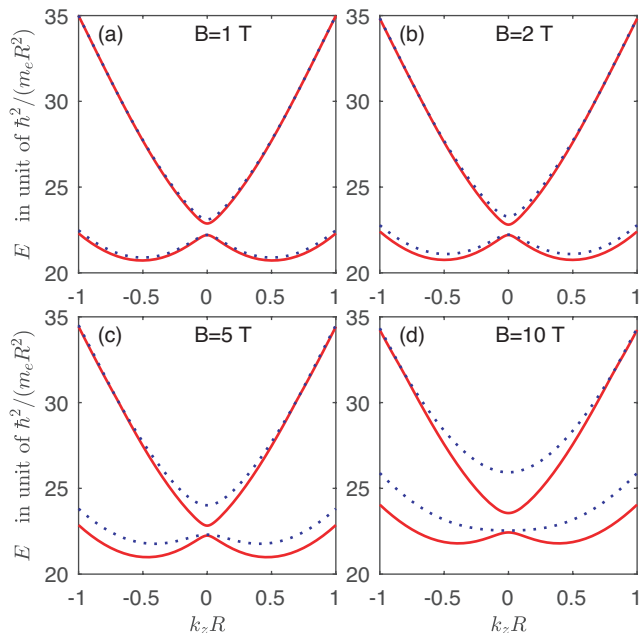


FIG. 2. The lowest four subband dispersions of the 1D hole gas under strong longitudinal magnetic fields. The results for $B = 1$ T (a), $B = 2$ T (b), $B = 5$ T (c), and $B = 10$ T (d).

hole can be well represented by the first and the third lowest subband dispersions, i.e., the solid lines given in Fig. 2. In particular, these two dispersions are well described by the following function relation

$$\frac{E}{\hbar^2/(m_e R^2)} = a k_z^2 R^2 + b \sigma^z k_z R + c \sigma^x + d, \quad (3)$$

where a , b , c , and d are dimensionless parameters to be determined in the following, and $\sigma^{x,z}$ are Pauli matrices introduced to mimic the two displaced parabolic curves with an anticrossing at $k_z R = 0$. Let us now explain how to determine these parameters. First, the parameter c is determined by the magnitude of the energy gap at the site $k_z R = 0$. Second, the parameters a , b , and d are determined by a second order polynomial curve fitting to one of the parabolic data shown in Fig. 2. For example, for the data at the magnetic field $B = 5$ T given in Fig. 2(c), we have $c \approx 0.29$ from the energy gap at $k_z R = 0$, and we also have $a \approx 6.47$, $b \approx 6.4$, and $d \approx 22.61$ by fitting to the left solid parabolic curve. It is obvious that the parameters a , b , c , and d have a dependence on the magnetic field B . We rewrite Eq. (3) in the more intuitional form

$$E = \frac{\hbar^2 k_z^2}{2m_h^*} + \alpha \sigma^z k_z + \frac{g_h^* \mu_B B}{2} \sigma^x + const., \quad (4)$$

where $m_h^* = m_e/(2a)$ can be regarded as the hole effective mass, $\alpha = b\hbar^2/(m_e R)$ is the strength of the ‘spin’-orbit coupling, and $g_h^* = 2c\hbar^2/(\mu_B B m_e R^2)$ is the effective g -factor of the hole ‘spin’. Note that we have used a strong magnetic field to split off the unwanted spin degree of

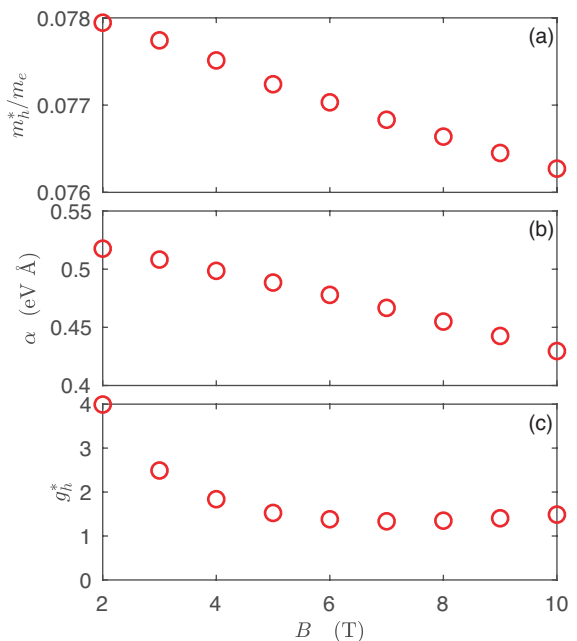


FIG. 3. The magnetic field dependence of the hole effective mass (a), the hole ‘spin’-orbit coupling (b), and the effective g -factor (c) of the hole ‘spin’. The field is applied along the nanowire.

freedom in the original two-fold degenerate hole subband dispersions, such that the operator σ^x here does not represent the real hole spin. It is more proper to regard σ^x as a pseudo spin, this is why we have added a single quote to the text ‘spin’.

We show the magnetic field dependences of the effective mass m_h^* , the ‘spin’-orbit coupling α , and the effective g -factor g_h^* of the hole ‘spin’ in Fig. 3. Note that the induced hole effective mass m_h^* in the cylindrical nanowire considered here has the same order of magnitude as that in the planar Ge quantum well [22, 44]. The induced spin-orbit coupling given in Eq. (4) is of the Rashba type [47], and its magnitude is in the order of several fractions of eV Å [see Fig. 3(b)]. In the magnetic field interval $2 \text{ T} < B < 10 \text{ T}$ considered here, both m_h^* and α decrease with the increase of the longitudinal magnetic field. Of course, the variations of m_h^* and α are small in this interval. While for the effective g -factor g_h^* , it only has a small dependence on the magnetic field in the large fields region [see Fig. 3(c)].

IV. 1D HOLE GAS IN A STRONG TRANSVERSE MAGNETIC FIELD

A strong transverse magnetic field $\mathbf{B} = (B, 0, 0)$ is certainly also feasible to split off the unwanted spin degeneracy in the subband dispersions of the 1D hole gas. Now the bare Zeeman term is written as $2\kappa\mu_B B J_x$, and the vector potential can be conveniently chosen as $\mathbf{A} = (0, 0, By)$. By choosing this gauge, the operator p_z

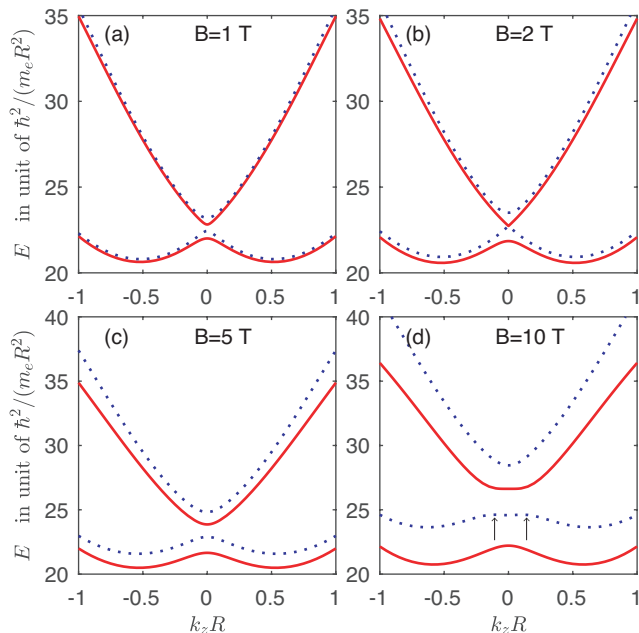


FIG. 4. The lowest four subband dispersions of the 1D hole gas under strong transverse magnetic fields. The results for $B = 1$ T (a), $B = 2$ T (b), $B = 5$ T (c), and $B = 10$ T (d). The two arrows in (d) mark the two very small anticrossings between the second and the third lowest subband dispersions.

in the hole Hamiltonian H is still a conserved quantity, and the subband dispersions can still be written $E_n(k_z)$. We rewrite the hole Hamiltonian in perturbative series with respect to the magnetic field $H = H_0 + H^{(p)}$, where $H^{(p)}$ is the perturbation Hamiltonian consisting of the bare Zeeman term plus all the orbital terms of the magnetic field (for details see appendix C). Note that the perturbation Hamiltonian in a transverse field is totally different from that in a longitudinal field.

We use the quasi-degenerate perturbation theory to calculate the lowest four subband dispersions of the 1D hole gas in this strong transverse magnetic field. The obtained results are explicitly shown in Fig. 4. Because of the large transverse effective hole g -factors at $k_z R = 0$ [24, 25], at the magnetic field $B \approx 2$ T, the second and the third lowest subband dispersions almost touch with each other at the site $k_z R = 0$ [see Fig. 4(b)]. For magnetic fields $B > 2$ T, there are two very small anticrossings between the second and the third lowest subband dispersions, where one anticrossing has a very small negative $k_z R$ value and the other anticrossing has a very small positive $k_z R$ value [this can be seen clearly when the magnetic field is large enough, e.g., see Fig. 4(d)].

If we ignore the potential consequences of the two very small anticrossings between the second and the third lowest subband dispersions, the first and the third lowest subband dispersions, i.e., the solid lines shown in Fig. 4, can still be approximately described by Eq. (4). Hence, we still can achieve a strong spin-orbit coupled 1D hole gas in a strong transverse magnetic field. We show the

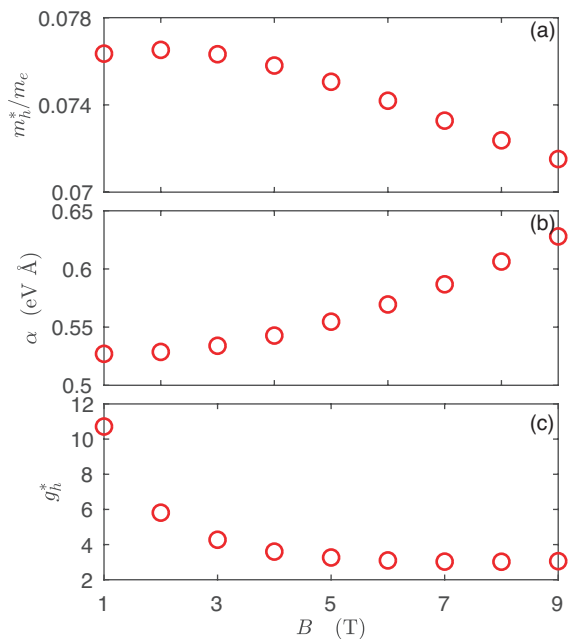


FIG. 5. The magnetic field dependence of the hole effective mass (a), the hole ‘spin’-orbit coupling (b), and the effective g -factor (c) of the hole ‘spin’. The field is applied perpendicular to the nanowire.

magnetic field dependences of the effective mass m_h^* , the ‘spin’-orbit coupling α , and the effective g -factor of the hole ‘spin’ in Fig. 5. We note that, different from the longitudinal magnetic field case, with the increase of the transverse magnetic field, the spin-orbit coupling α increases instead [see Fig. 5(b)].

Because of the existence of the two very small anticrossings between the second and third lowest subband dispersions of the hole gas in a strong transverse magnetic field, the longitudinal magnetic field may be more proper for achieving the strong ‘spin’-orbit coupled 1D hole gas.

V. SUMMARY

Due to the reason that the Hamiltonian of the hole in a cylindrical nanowire has both the time reversal symmetry and the spin-rotation symmetry, such that there is a spin degeneracy in the induced hole subband dispersions. In this paper, we unambiguously show that a strong spin-orbit coupled 1D hole gas is indeed realizable via applying a strong magnetic field to lift the spin degeneracy in the original two-fold degenerate hole subbands. The induced subband dispersion governing the low-energy physics of the hole gas have a very simple form, which is exactly identical to that of the well studied strong spin-orbit coupled 1D electron gas. Our study indicates that the strong spin-orbit coupled 1D hole gas may have broad application prospects as well as the well-studied 1D electron gas.

ACKNOWLEDGEMENTS

This work is supported by the National Natural Science Foundation of China Grant No. 11404020, the

Project from the Department of Education of Hebei Province Grant No. QN2019057, and the Starting up Foundation from Yanshan University Grant No. BL18043.

Appendix A: Basis states for quasi-degenerate perturbation calculations

For wave vectors in the interval $|k_z R| < 1$, the lowest two subbands are approximately separated from the other higher subbands. The basis states of the quasi-degenerate Hilbert subspace read

$$|1\rangle = \begin{pmatrix} \Psi_{I,1}(r)e^{-i\varphi} \\ \Psi_{I,2}(r) \\ \Psi_{I,3}(r)e^{i\varphi} \\ \Psi_{I,4}(r)e^{2i\varphi} \end{pmatrix}, |2\rangle = \begin{pmatrix} -\Psi_{I,4}^*(r)e^{-2i\varphi} \\ \Psi_{I,3}^*(r)e^{-i\varphi} \\ -\Psi_{I,2}^*(r) \\ \Psi_{I,1}^*(r)e^{i\varphi} \end{pmatrix}, |3\rangle = \begin{pmatrix} \Psi_{II,1}(r)e^{-i\varphi} \\ \Psi_{II,2}(r) \\ \Psi_{II,3}(r)e^{i\varphi} \\ \Psi_{II,4}(r)e^{2i\varphi} \end{pmatrix}, |4\rangle = \begin{pmatrix} -\Psi_{II,4}^*(r)e^{-2i\varphi} \\ \Psi_{II,3}^*(r)e^{-i\varphi} \\ -\Psi_{II,2}^*(r) \\ \Psi_{II,1}^*(r)e^{i\varphi} \end{pmatrix}. \quad (\text{A1})$$

In consistence with our preceding notations, here $|1\rangle \equiv \Psi_{1,k_z,\uparrow}$, $|2\rangle \equiv \Psi_{1,k_z,\downarrow}$, $|3\rangle \equiv \Psi_{2,k_z,\uparrow}$, and $|4\rangle \equiv \Psi_{2,k_z,\downarrow}$.

Appendix B: Longitudinal magnetic field case

When the magnetic field is applied longitudinally, the hole Hamiltonian can be written in perturbation series

$$H = H_0 + H^{(p_1)} + H^{(p_2)} + H^{(p_3)} + H^{(p_4)} + H^{(p_5)}, \quad (\text{B1})$$

where H_0 is the zero-order diagonal Hamiltonian, and $H^{(p_i)}$ ($i = 1, \dots, 5$) are the perturbation Hamiltonians. The explicit form of each perturbation term $H^{(p_i)}$ is given in the following corresponding subsection.

1. Perturbation term I: $H^{(p_1)} = 2\kappa\mu_B B J_z$

The matrix elements of the perturbation term $H^{(p_1)}$ read

$$\begin{aligned} H_{11}^{(p_1)} &= 4\pi\kappa\mu_B B \int_0^R dr r \left(\frac{3}{2} |\Psi_{I,1}(r)|^2 + \frac{1}{2} |\Psi_{I,2}(r)|^2 - \frac{1}{2} |\Psi_{I,3}(r)|^2 - \frac{3}{2} |\Psi_{I,4}(r)|^2 \right), \\ H_{12}^{(p_1)} &= 0, \\ H_{13}^{(p_1)} &= 4\pi\kappa\mu_B B \int_0^R dr r \left(\frac{3}{2} \Psi_{I,1}^*(r) \Psi_{II,1}(r) + \frac{1}{2} \Psi_{I,2}^*(r) \Psi_{II,2}(r) - \frac{1}{2} \Psi_{I,3}^*(r) \Psi_{II,3}(r) - \frac{3}{2} \Psi_{I,4}^*(r) \Psi_{II,4}(r) \right), \\ H_{14}^{(p_1)} &= 0, \\ H_{22}^{(p_1)} &= -H_{11}^{(p_1)}, \\ H_{23}^{(p_1)} &= 0, \\ H_{24}^{(p_1)} &= -\left(H_{13}^{(p_1)} \right)^*, \\ H_{33}^{(p_1)} &= 4\pi\kappa\mu_B B \int_0^R dr r \left(\frac{3}{2} |\Psi_{II,1}(r)|^2 + \frac{1}{2} |\Psi_{II,2}(r)|^2 - \frac{1}{2} |\Psi_{II,3}(r)|^2 - \frac{3}{2} |\Psi_{II,4}(r)|^2 \right), \\ H_{34}^{(p_1)} &= 0, \\ H_{44}^{(p_1)} &= -H_{33}^{(p_1)}. \end{aligned} \quad (\text{B2})$$

2. Perturbation term II: $H^{(p_2)}$

In this subsection, the perturbation term reads

$$H^{(p_2)} = -i\mu_B B \partial_\varphi \begin{pmatrix} \gamma_1 + \gamma_s & 0 & 0 & 0 \\ 0 & \gamma_1 - \gamma_s & 0 & 0 \\ 0 & 0 & \gamma_1 - \gamma_s & 0 \\ 0 & 0 & 0 & \gamma_1 + \gamma_s \end{pmatrix}. \quad (\text{B3})$$

The matrix elements of the perturbation term read

$$\begin{aligned} H_{11}^{(p_2)} &= 2\pi\mu_B B \int_0^R dr r \left(-(\gamma_1 + \gamma_s)|\Psi_{I,1}(r)|^2 + (\gamma_1 - \gamma_s)|\Psi_{I,3}(r)|^2 + 2(\gamma_1 + \gamma_s)|\Psi_{I,4}(r)|^2 \right), \\ H_{12}^{(p_2)} &= 0, \\ H_{13}^{(p_2)} &= 2\pi\mu_B B \int_0^R dr r \left(-(\gamma_1 + \gamma_s)\Psi_{I,1}^*(r)\Psi_{II,1}(r) + (\gamma_1 - \gamma_s)\Psi_{I,3}^*(r)\Psi_{II,3}(r) + 2(\gamma_1 + \gamma_s)\Psi_{I,4}^*(r)\Psi_{II,4}(r) \right) \end{aligned} \quad (\text{B4})$$

$$\begin{aligned} H_{14}^{(p_2)} &= 0, \\ H_{22}^{(p_2)} &= -H_{11}^{(p_2)}, \\ H_{23}^{(p_2)} &= 0, \\ H_{24}^{(p_2)} &= -\left(H_{13}^{(p_2)}\right)^*, \\ H_{33}^{(p_2)} &= 2\pi\mu_B B \int_0^R dr r \left(-(\gamma_1 + \gamma_s)|\Psi_{II,1}(r)|^2 + (\gamma_1 - \gamma_s)|\Psi_{II,3}(r)|^2 + 2(\gamma_1 + \gamma_s)|\Psi_{II,4}(r)|^2 \right), \end{aligned} \quad (\text{B5})$$

$$\begin{aligned} H_{34}^{(p_2)} &= 0, \\ H_{44}^{(p_2)} &= -H_{33}^{(p_2)}. \end{aligned} \quad (\text{B6})$$

3. Perturbation term III: $H^{(p_3)}$

In this subsection, the perturbation term reads

$$H^{(p_3)} = -\sqrt{3}\gamma_s\mu_B B \begin{pmatrix} 0 & -ik_z r e^{-i\varphi} & e^{-2i\varphi}(-r\partial_r + i\partial_\varphi) & 0 \\ ik_z r e^{i\varphi} & 0 & 0 & e^{-2i\varphi}(-r\partial_r + i\partial_\varphi) \\ e^{2i\varphi}(r\partial_r + i\partial_\varphi) & 0 & 0 & ik_z r e^{-i\varphi} \\ 0 & e^{2i\varphi}(r\partial_r + i\partial_\varphi) & -ik_z r e^{i\varphi} & 0 \end{pmatrix}. \quad (\text{B7})$$

The matrix elements of the perturbation term read

$$\begin{aligned}
H_{11}^{(p3)} &= 2\pi\sqrt{3}\gamma_s\mu_B B \int_0^R dr r \left(ik_z r \Psi_{I,1}^*(r) \Psi_{I,2}(r) - ik_z r \Psi_{I,2}^*(r) \Psi_{I,1}(r) - ik_z r \Psi_{I,3}^*(r) \Psi_{I,4}(r) \right. \\
&\quad + ik_z r \Psi_{I,4}^*(r) \Psi_{I,3}(r) + \Psi_{I,1}^*(r) (r\partial_r + 1) \Psi_{I,3}(r) + \Psi_{I,1}(r) (r\partial_r + 1) \Psi_{I,3}^*(r) \\
&\quad \left. + \Psi_{I,2}^*(r) (r\partial_r + 2) \Psi_{I,4}(r) + \Psi_{I,2}(r) (r\partial_r + 2) \Psi_{I,4}^*(r) \right), \\
H_{12}^{(p3)} &= 0, \\
H_{13}^{(p3)} &= 2\pi\sqrt{3}\gamma_s\mu_B B \int_0^R dr r \left(ik_z r \Psi_{I,1}^*(r) \Psi_{II,2}(r) - ik_z r \Psi_{I,2}^*(r) \Psi_{II,1}(r) - ik_z r \Psi_{I,3}^*(r) \Psi_{II,4}(r) \right. \\
&\quad + ik_z r \Psi_{I,4}^*(r) \Psi_{II,3}(r) + \Psi_{I,1}^*(r) (r\partial_r + 1) \Psi_{II,3}(r) + \Psi_{II,1}(r) (r\partial_r + 1) \Psi_{I,3}^*(r) \\
&\quad \left. + \Psi_{I,2}^*(r) (r\partial_r + 2) \Psi_{II,4}(r) + \Psi_{II,2}(r) (r\partial_r + 2) \Psi_{I,4}^*(r) \right), \\
H_{14}^{(p3)} &= 0, \\
H_{22}^{(p3)} &= 2\pi\sqrt{3}\gamma_s\mu_B B \int_0^R dr r \left(ik_z r \Psi_{I,2}(r) \Psi_{I,1}^*(r) - ik_z r \Psi_{I,1}(r) \Psi_{I,2}^*(r) - ik_z r \Psi_{I,4}(r) \Psi_{I,3}^*(r) \right. \\
&\quad + ik_z r \Psi_{I,3}(r) \Psi_{I,4}^*(r) - \Psi_{I,1}(r) (r\partial_r + 1) \Psi_{I,3}^*(r) - \Psi_{I,1}^*(r) (r\partial_r + 1) \Psi_{I,3}(r) \\
&\quad \left. - \Psi_{I,2}(r) (r\partial_r + 2) \Psi_{I,4}^*(r) - \Psi_{I,2}^*(r) (r\partial_r + 2) \Psi_{I,4}(r) \right), \\
H_{23}^{(p3)} &= 0, \\
H_{24}^{(p3)} &= -2\pi\sqrt{3}\gamma_s\mu_B B \int_0^R dr r \left(ik_z r \Psi_{I,1}(r) \Psi_{II,2}^*(r) - ik_z r \Psi_{I,2}(r) \Psi_{II,1}^*(r) - ik_z r \Psi_{I,3}(r) \Psi_{II,4}^*(r) \right. \\
&\quad + ik_z r \Psi_{I,4}(r) \Psi_{II,3}^*(r) + \Psi_{II,2}^*(r) (r\partial_r + 2) \Psi_{I,4}(r) + \Psi_{II,1}^*(r) (r\partial_r + 1) \Psi_{I,3}(r) \\
&\quad \left. + \Psi_{I,2}(r) (r\partial_r + 2) \Psi_{II,4}^*(r) + \Psi_{I,1}(r) (r\partial_r + 1) \Psi_{II,3}^*(r) \right), \\
H_{33}^{(p3)} &= 2\pi\sqrt{3}\gamma_s\mu_B B \int_0^R dr r \left(ik_z r \Psi_{II,1}^*(r) \Psi_{II,2}(r) - ik_z r \Psi_{II,2}^*(r) \Psi_{II,1}(r) - ik_z r \Psi_{II,3}^*(r) \Psi_{II,4}(r) \right. \\
&\quad + ik_z r \Psi_{II,4}^*(r) \Psi_{II,3}(r) + \Psi_{II,1}^*(r) (r\partial_r + 1) \Psi_{II,3}(r) + \Psi_{II,1}(r) (r\partial_r + 1) \Psi_{II,3}^*(r) \\
&\quad \left. + \Psi_{II,2}^*(r) (r\partial_r + 2) \Psi_{II,4}(r) + \Psi_{II,2}(r) (r\partial_r + 2) \Psi_{II,4}^*(r) \right), \\
H_{34}^{(p3)} &= 0, \\
H_{44}^{(p3)} &= 2\pi\sqrt{3}\gamma_s\mu_B B \int_0^R dr r \left(ik_z r \Psi_{II,2}(r) \Psi_{II,1}^*(r) - ik_z r \Psi_{II,1}(r) \Psi_{II,2}^*(r) - ik_z r \Psi_{II,4}(r) \Psi_{II,3}^*(r) \right. \\
&\quad + ik_z r \Psi_{II,3}(r) \Psi_{II,4}^*(r) - \Psi_{II,1}(r) (r\partial_r + 1) \Psi_{II,3}^*(r) - \Psi_{II,1}^*(r) (r\partial_r + 1) \Psi_{II,3}(r) \\
&\quad \left. - \Psi_{II,2}(r) (r\partial_r + 2) \Psi_{II,4}^*(r) - \Psi_{II,2}^*(r) (r\partial_r + 2) \Psi_{II,4}(r) \right). \tag{B8}
\end{aligned}$$

4. Perturbation term IV: $H_l^{(p4)}$

In this subsection, the perturbation term reads

$$H^{(p4)} = \left(\gamma_1 + \frac{5}{2}\gamma_s \right) \frac{e^2 B^2 r^2}{8m_e}. \tag{B9}$$

The matrix elements of the perturbation term read

$$\begin{aligned}
H_{11}^{(p_4)} &= 2\pi(\gamma_1 + \frac{5}{2}\gamma_s) \frac{e^2 B^2}{8m_e} \int_0^R dr r^3 \left(|\Psi_{I,1}(r)|^2 + |\Psi_{I,2}(r)|^2 + |\Psi_{I,3}(r)|^2 + |\Psi_{I,4}(r)|^2 \right), \\
H_{12}^{(p_4)} &= 0, \\
H_{13}^{(p_4)} &= 2\pi \left(\gamma_1 + \frac{5}{2}\gamma_s \right) \frac{e^2 B^2}{8m_e} \int_0^R dr r^3 \left(\Psi_{I,1}^*(r) \Psi_{II,1}(r) + \Psi_{I,2}^*(r) \Psi_{II,2}(r) + \Psi_{I,3}^*(r) \Psi_{II,3}(r) + \Psi_{I,4}^*(r) \Psi_{II,4}(r) \right), \\
H_{14}^{(p_4)} &= 0, \\
H_{22}^{(p_4)} &= H_{11}^{(p_4)}, \\
H_{23}^{(p_4)} &= 0, \\
H_{24}^{(p_4)} &= \left(H_{13}^{(p_4)} \right)^*, \\
H_{33}^{(p_4)} &= 2\pi(\gamma_1 + \frac{5}{2}\gamma_s) \frac{e^2 B^2}{8m_e} \int_0^R dr r^3 \left(|\Psi_{II,1}(r)|^2 + |\Psi_{II,2}(r)|^2 + |\Psi_{II,3}(r)|^2 + |\Psi_{II,4}(r)|^2 \right), \\
H_{34}^{(p_4)} &= 0, \\
H_{44}^{(p_4)} &= H_{33}^{(p_4)}.
\end{aligned} \tag{B10}$$

5. Perturbation term V: $H_l^{(p_5)}$

In this subsection, the perturbation term reads

$$H^{(p_5)} = -\frac{\gamma_s e^2 B^2 r^2}{4m_e} \begin{pmatrix} \frac{3}{4} & 0 & -\frac{\sqrt{3}}{2} e^{-2i\varphi} & 0 \\ 0 & \frac{7}{4} & 0 & -\frac{\sqrt{3}}{2} e^{-2i\varphi} \\ -\frac{\sqrt{3}}{2} e^{2i\varphi} & 0 & \frac{7}{4} & 0 \\ 0 & -\frac{\sqrt{3}}{2} e^{2i\varphi} & 0 & \frac{3}{4} \end{pmatrix}. \tag{B11}$$

The matrix elements of the perturbation term read

$$\begin{aligned}
H_{11}^{(p_5)} &= -\frac{2\pi\gamma_s e^2 B^2}{4m_e} \int_0^R dr r^3 \left(-\frac{\sqrt{3}}{2} \Psi_{I,1}^*(r) \Psi_{I,3}(r) - \frac{\sqrt{3}}{2} \Psi_{I,3}^*(r) \Psi_{I,1}(r) - \frac{\sqrt{3}}{2} \Psi_{I,2}^*(r) \Psi_{I,4}(r) - \frac{\sqrt{3}}{2} \Psi_{I,4}^*(r) \Psi_{I,2}(r) \right. \\
&\quad \left. + \frac{3}{4} |\Psi_{I,1}(r)|^2 + \frac{7}{4} |\Psi_{I,2}(r)|^2 + \frac{7}{4} |\Psi_{I,3}(r)|^2 + \frac{3}{4} |\Psi_{I,4}(r)|^2 \right), \\
H_{12}^{(p_5)} &= 0, \\
H_{13}^{(p_5)} &= -\frac{2\pi\gamma_s e^2 B^2}{4m_e} \int_0^R dr r^3 \left(-\frac{\sqrt{3}}{2} \Psi_{I,1}^*(r) \Psi_{II,3}(r) - \frac{\sqrt{3}}{2} \Psi_{I,3}^*(r) \Psi_{II,1}(r) - \frac{\sqrt{3}}{2} \Psi_{I,2}^*(r) \Psi_{II,4}(r) \right. \\
&\quad \left. - \frac{\sqrt{3}}{2} \Psi_{I,4}^*(r) \Psi_{II,2}(r) + \frac{3}{4} \Psi_{I,1}^*(r) \Psi_{II,1}(r) + \frac{7}{4} \Psi_{I,2}^*(r) \Psi_{II,2}(r) + \frac{7}{4} \Psi_{I,3}^*(r) \Psi_{II,3}(r) + \frac{3}{4} \Psi_{I,4}^*(r) \Psi_{II,4}(r) \right), \\
H_{14}^{(p_5)} &= 0, \\
H_{22}^{(p_5)} &= H_{11}^{(p_5)}, \\
H_{23}^{(p_5)} &= 0, \\
H_{24}^{(p_5)} &= \left(H_{13}^{(p_5)} \right)^*, \\
H_{33}^{(p_5)} &= -\frac{2\pi\gamma_s e^2 B^2}{4m_e} \int_0^R dr r^3 \left(-\frac{\sqrt{3}}{2} \Psi_{II,1}^*(r) \Psi_{II,3}(r) - \frac{\sqrt{3}}{2} \Psi_{II,3}^*(r) \Psi_{II,1}(r) - \frac{\sqrt{3}}{2} \Psi_{II,2}^*(r) \Psi_{II,4}(r) \right. \\
&\quad \left. - \frac{\sqrt{3}}{2} \Psi_{II,4}^*(r) \Psi_{II,2}(r) + \frac{3}{4} |\Psi_{II,1}(r)|^2 + \frac{7}{4} |\Psi_{II,2}(r)|^2 + \frac{7}{4} |\Psi_{II,3}(r)|^2 + \frac{3}{4} |\Psi_{II,4}(r)|^2 \right), \\
H_{34}^{(p_5)} &= 0, \\
H_{44}^{(p_5)} &= H_{33}^{(p_5)}.
\end{aligned} \tag{B12}$$

(B13)

Appendix C: Transverse magnetic field case

When the magnetic field is applied transversely, the hole Hamiltonian can be written in perturbation series

$$H = H_0 + H^{(p1)} + H^{(p2)} + H^{(p3)} + H^{(p4)}, \quad (\text{C1})$$

where H_0 is the zero-order diagonal Hamiltonian, and $H_l^{(p_i)}$ ($i = 1, \dots, 4$) are the perturbation Hamiltonians. The explicit form of each perturbation term $H^{(p_i)}$ is given in the following corresponding subsection.

1. Perturbation term I: $H^{(p1)} = 2\kappa\mu_B B J_x$

The matrix elements of the perturbation term read

$$\begin{aligned} H_{11}^{(p1)} &= 0, \\ H_{12}^{(p1)} &= 4\pi\kappa\mu_B B \int_0^R dr r \left(\sqrt{3}\Psi_{I,1}^*(r)\Psi_{I,3}^*(r) - \Psi_{I,2}^*(r)\Psi_{I,2}^*(r) \right), \\ H_{13}^{(p1)} &= 0, \\ H_{14}^{(p1)} &= 4\pi\kappa\mu_B B \int_0^R dr r \left(\frac{\sqrt{3}}{2}\Psi_{I,1}^*(r)\Psi_{II,3}^*(r) + \frac{\sqrt{3}}{2}\Psi_{I,3}^*(r)\Psi_{II,1}^*(r) - \Psi_{I,2}^*(r)\Psi_{II,2}^*(r) \right), \\ H_{22}^{(p1)} &= 0, \\ H_{23}^{(p1)} &= \left(H_{14}^{(p1)} \right)^*, \\ H_{24}^{(p1)} &= 0, \\ H_{33}^{(p1)} &= 0, \\ H_{34}^{(p1)} &= 4\pi\kappa\mu_B B \int_0^R dr r \left(\sqrt{3}\Psi_{II,1}^*(r)\Psi_{II,3}^*(r) - \Psi_{II,2}^*(r)\Psi_{II,2}^*(r) \right), \\ H_{44}^{(p1)} &= 0. \end{aligned} \quad (\text{C2})$$

2. Perturbation term II: $H^{(p2)}$

In this subsection, the perturbation term reads

$$H^{(p2)} = 2\sqrt{3}\gamma_s\mu_B B \begin{pmatrix} 0 & e^{-i\varphi} \sin \varphi (ir\partial_r + \partial_\varphi) + \frac{1}{2} & 0 & 0 \\ e^{i\varphi} \sin \varphi (ir\partial_r - \partial_\varphi) - \frac{1}{2} & 0 & 0 & 0 \\ 0 & 0 & 0 & e^{-i\varphi} \sin \varphi (-ir\partial_r - \partial_\varphi) - \frac{1}{2} \\ 0 & 0 & e^{i\varphi} \sin \varphi (-ir\partial_r + \partial_\varphi) + \frac{1}{2} & 0 \end{pmatrix}. \quad (\text{C3})$$

The matrix elements of the perturbation term read

$$\begin{aligned}
H_{11}^{(p_2)} &= 0, \\
H_{12}^{(p_2)} &= 4\pi\sqrt{3}\gamma_s\mu_B B \int_0^R dr r \left(\Psi_{I,1}^*(r)(r\partial_r + 1)\Psi_{I,3}^*(r) - \Psi_{I,2}^*(r)(r\partial_r + 2)\Psi_{I,4}^*(r) - \Psi_{I,1}^*(r)\Psi_{I,3}^*(r) \right), \\
H_{13}^{(p_2)} &= 0, \\
H_{14}^{(p_2)} &= 2\pi\sqrt{3}\gamma_s\mu_B B \int_0^R dr r \left(\Psi_{I,1}^*(r)(r\partial_r + 1)\Psi_{II,3}^*(r) + \Psi_{II,1}^*(r)(r\partial_r + 1)\Psi_{I,3}^*(r) - \Psi_{I,2}^*(r)(r\partial_r + 2)\Psi_{II,4}^*(r) \right. \\
&\quad \left. - \Psi_{II,2}^*(r)(r\partial_r + 2)\Psi_{I,4}^*(r) - \Psi_{I,1}^*(r)\Psi_{II,3}^*(r) - \Psi_{II,1}^*(r)\Psi_{I,3}^*(r) \right), \\
H_{22}^{(p_2)} &= 0, \\
H_{23}^{(p_2)} &= \left(H_{14}^{(p_2)} \right)^*, \\
H_{24}^{(p_2)} &= 0, \\
H_{33}^{(p_2)} &= 0, \\
H_{34}^{(p_2)} &= 4\pi\sqrt{3}\gamma_s\mu_B B \int_0^R dr r \left(\Psi_{II,1}^*(r)(r\partial_r + 1)\Psi_{II,3}^*(r) - \Psi_{II,2}^*(r)(r\partial_r + 2)\Psi_{II,4}^*(r) - \Psi_{II,1}^*(r)\Psi_{II,3}^*(r) \right), \\
H_{44}^{(p_2)} &= 0.
\end{aligned} \tag{C4}$$

3. Perturbation term III: $H^{(p_3)}$

In this subsection, the perturbation term reads

$$H^{(p_3)} = \frac{e^2 B^2 r^2 \sin^2 \varphi}{2m_e} \begin{pmatrix} \gamma_1 - 2\gamma_s & 0 & 0 & 0 \\ 0 & \gamma_1 + 2\gamma_s & 0 & 0 \\ 0 & 0 & \gamma_1 + 2\gamma_s & 0 \\ 0 & 0 & 0 & \gamma_1 - 2\gamma_s \end{pmatrix}. \tag{C5}$$

The matrix elements of the perturbation term read

$$\begin{aligned}
H_{11}^{(p_3)} &= \frac{\pi e^2 B^2}{2m_e} \int_0^R dr r^3 \left((\gamma_1 - 2\gamma_s)|\Psi_{I,1}(r)|^2 + (\gamma_1 + 2\gamma_s)|\Psi_{I,2}(r)|^2 + (\gamma_1 + 2\gamma_s)|\Psi_{I,3}(r)|^2 + (\gamma_1 - 2\gamma_s)|\Psi_{I,4}(r)|^2 \right), \\
H_{12}^{(p_3)} &= 0, \\
H_{13}^{(p_3)} &= \frac{\pi e^2 B^2}{2m_e} \int_0^R dr r^3 \left((\gamma_1 - 2\gamma_s)\Psi_{I,1}^*(r)\Psi_{II,1}(r) + (\gamma_1 + 2\gamma_s)\Psi_{I,2}^*(r)\Psi_{II,2}(r) \right. \\
&\quad \left. + (\gamma_1 + 2\gamma_s)\Psi_{I,3}^*(r)\Psi_{II,3}(r) + (\gamma_1 - 2\gamma_s)\Psi_{I,4}^*(r)\Psi_{II,4}(r) \right), \\
H_{14}^{(p_3)} &= 0, \\
H_{22}^{(p_3)} &= H_{11}^{(p_3)}, \\
H_{23}^{(p_3)} &= 0, \\
H_{24}^{(p_3)} &= \left(H_{13}^{(p_3)} \right)^*, \\
H_{33}^{(p_3)} &= \frac{\pi e^2 B^2}{2m_e} \int_0^R dr r^3 \left((\gamma_1 - 2\gamma_s)|\Psi_{II,1}(r)|^2 + (\gamma_1 + 2\gamma_s)|\Psi_{II,2}(r)|^2 \right. \\
&\quad \left. + (\gamma_1 + 2\gamma_s)|\Psi_{II,3}(r)|^2 + (\gamma_1 - 2\gamma_s)|\Psi_{II,4}(r)|^2 \right), \\
H_{34}^{(p_3)} &= 0, \\
H_{44}^{(p_3)} &= H_{33}^{(p_3)}.
\end{aligned} \tag{C6}$$

4. Perturbation term IV: $H^{(p_4)}$

In this subsection, the perturbation term reads

$$H^{(p_4)} = 2\mu_B B k_z r \sin \varphi \begin{pmatrix} \gamma_1 - 2\gamma_s & 0 & 0 & 0 \\ 0 & \gamma_1 + 2\gamma_s & 0 & 0 \\ 0 & 0 & \gamma_1 + 2\gamma_s & 0 \\ 0 & 0 & 0 & \gamma_1 - 2\gamma_s \end{pmatrix}. \quad (\text{C7})$$

The matrix elements of the perturbation term read

$$\begin{aligned} H_{11}^{(p_4)} &= 0, \\ H_{12}^{(p_4)} &= 0, \\ H_{13}^{(p_4)} &= 0, \\ H_{14}^{(p_4)} &= -2i\pi\mu_B B k_z \int_0^R dr r^2 \left(-(\gamma_1 - 2\gamma_s) \Psi_{I,1}^*(r) \Psi_{II,4}^*(r) + (\gamma_1 + 2\gamma_s) \Psi_{I,2}^*(r) \Psi_{II,3}^*(r) \right. \\ &\quad \left. - (\gamma_1 + 2\gamma_s) \Psi_{I,3}^*(r) \Psi_{II,2}^*(r) + (\gamma_1 - 2\gamma_s) \Psi_{I,4}^*(r) \Psi_{II,1}^*(r) \right), \\ H_{22}^{(p_4)} &= 0, \\ H_{23}^{(p_4)} &= - \left(H_{14}^{(p_4)} \right)^*, \\ H_{24}^{(p_4)} &= 0, \\ H_{33}^{(p_4)} &= 0, \\ H_{34}^{(p_4)} &= 0, \\ H_{44}^{(p_4)} &= 0. \end{aligned} \quad (\text{C8})$$

-
- [1] R. Hanson, L. P. Kouwenhoven, J. R. Petta, S. Tarucha, and L. M. K. Vandersypen, Spins in few-electron quantum dots, *Rev. Mod. Phys.* **79**, 1217 (2007).
 - [2] L. M. K. Vandersypen and M. A. Eriksson, Quantum computing with semiconductor spins, *Physics Today* **72**, 38 (2019).
 - [3] D. Loss and D. P. DiVincenzo, Quantum computation with quantum dots, *Phys. Rev. A* **57**, 120 (1998).
 - [4] G. Scappucci, C. Kloeffel, F. A. Zwanenburg, D. Loss, M. Myronov, J.-J. Zhang, S. De Franceschi, G. Katsaros, and M. Veldhorst, The germanium quantum information route, *Nature Reviews Materials* [10.1038/s41578-020-00262-z](https://doi.org/10.1038/s41578-020-00262-z) (2020).
 - [5] J. M. Luttinger and W. Kohn, Motion of electrons and holes in perturbed periodic fields, *Phys. Rev.* **97**, 869 (1955).
 - [6] J. M. Luttinger, Quantum theory of cyclotron resonance in semiconductors: General theory, *Phys. Rev.* **102**, 1030 (1956).
 - [7] D. V. Bulaev and D. Loss, Electric dipole spin resonance for heavy holes in quantum dots, *Phys. Rev. Lett.* **98**, 097202 (2007).
 - [8] Z. Wang, E. Marcellina, A. R. Hamilton, J. H. Cullen, S. Rogge, J. Salfi, and D. Culcer, Optimal operation points for ultrafast, highly coherent ge hole spin-orbit qubits, *npj Quantum Information* **7**, 54 (2021).
 - [9] N. W. Hendrickx, W. I. L. Lawrie, L. Petit, A. Sammak, G. Scappucci, and M. Veldhorst, A single-hole spin qubit, *Nature Communications* **11**, 3478 (2020).
 - [10] N. W. Hendrickx, D. P. Franke, A. Sammak, G. Scappucci, and M. Veldhorst, Fast two-qubit logic with holes in germanium, *Nature* **577**, 487 (2020).
 - [11] S. Roddaro, A. Fuhrer, P. Brusheim, C. Fasth, H. Q. Xu, L. Samuelson, J. Xiang, and C. M. Lieber, Spin states of holes in Ge/Si nanowire quantum dots, *Phys. Rev. Lett.* **101**, 186802 (2008).
 - [12] A. P. Higginbotham, F. Kuemmeth, T. W. Larsen, M. Fitzpatrick, J. Yao, H. Yan, C. M. Lieber, and C. M. Marcus, Antilocalization of coulomb blockade in a ge/si nanowire, *Phys. Rev. Lett.* **112**, 216806 (2014).
 - [13] F. N. M. Froning, L. C. Camenzind, O. A. H. van der Molen, A. Li, E. P. A. M. Bakkers, D. M. Zumbühl, and F. R. Braakman, Ultrafast hole spin qubit with gate-tunable spin-orbit switch functionality, *Nature Nanotechnology* **16**, 308 (2021).
 - [14] F. Gao, J.-H. Wang, H. Watzinger, H. Hu, M. J. Rančić, J.-Y. Zhang, T. Wang, Y. Yao, G.-L. Wang, J. Kukučka, L. Vukušić, C. Kloeffel, D. Loss, F. Liu, G. Katsaros, and J.-J. Zhang, Site-controlled uniform ge/si hut wires with electrically tunable spin-orbit coupling, *Advanced Materials* **32**, 1906523 (2020).
 - [15] T. Zhang, H. Liu, F. Gao, G. Xu, K. Wang, X. Zhang,

- G. Cao, T. Wang, J. Zhang, X. Hu, H.-O. Li, and G.-P. Guo, Anisotropic g -factor and spin-orbit field in a germanium hut wire double quantum dot, *Nano Letters* **21**, 3835 (2021).
- [16] C. Kloeffel, M. Trif, P. Stano, and D. Loss, Circuit qed with hole-spin qubits in ge/si nanowire quantum dots, *Phys. Rev. B* **88**, 241405 (2013).
- [17] H. Watzinger, J. Kukučka, L. Vukušić, F. Gao, T. Wang, F. Schäffler, J.-J. Zhang, and G. Katsaros, A germanium hole spin qubit, *Nature Communications* **9**, 3902 (2018).
- [18] M. Brauns, J. Ridderbos, A. Li, E. P. A. M. Bakkers, W. G. van der Wiel, and F. A. Zwanenburg, Anisotropic pauli spin blockade in hole quantum dots, *Phys. Rev. B* **94**, 041411 (2016).
- [19] H. Watzinger, C. Kloeffel, L. Vukušić, M. D. Rossell, V. Sessi, J. Kukučka, R. Kirchschrager, E. Lausecker, A. Truhlar, M. Glaser, A. Rastelli, A. Fuhrer, D. Loss, and G. Katsaros, Heavy-hole states in germanium hut wires, *Nano Letters* **16**, 6879 (2016).
- [20] P. M. Mutter and G. Burkard, Cavity control over heavy-hole spin qubits in inversion-symmetric crystals, *Phys. Rev. B* **102**, 205412 (2020).
- [21] F. N. M. Froning, M. J. Rančić, B. Hetényi, S. Bosco, M. K. Rehmann, A. Li, E. P. A. M. Bakkers, F. A. Zwanenburg, D. Loss, D. M. Zumbühl, and F. R. Braakman, Strong spin-orbit interaction and g -factor renormalization of hole spins in ge/si nanowire quantum dots, *Phys. Rev. Research* **3**, 013081 (2021).
- [22] L. A. Terrazos, E. Marcellina, Z. Wang, S. N. Copper-smith, M. Friesen, A. R. Hamilton, X. Hu, B. Koiller, A. L. Saraiva, D. Culcer, and R. B. Capaz, Theory of hole-spin qubits in strained germanium quantum dots, *Phys. Rev. B* **103**, 125201 (2021).
- [23] R. Winkler, *Spin-Orbit Effects in Two-Dimensional Electron and Hole Systems* (Springer, Berlin, 2003).
- [24] C. Kloeffel, M. Trif, and D. Loss, Strong spin-orbit interaction and helical hole states in ge/si nanowires, *Phys. Rev. B* **84**, 195314 (2011).
- [25] R. Li, Low-energy subband wave-functions and effective g -factor of one-dimensional hole gas, *Journal of Physics: Condensed Matter* (2021).
- [26] R. Li, Energy spectrum, the spin polarization, and the optical selection rules of the kronigpenney superlattice model with spin-orbit coupling, *Phys. Rev. B* **97**, 085430 (2018).
- [27] R. Li, Z. H. Liu, Y. Wu, and C. S. Liu, The impacts of the quantum-dot confining potential on the spin-orbit effect, *Sci Rep* **8**, 7400 (2018).
- [28] M. Trif, V. N. Golovach, and D. Loss, Spin dynamics in inas nanowire quantum dots coupled to a transmission line, *Phys. Rev. B* **77**, 045434 (2008).
- [29] R. Li, J. Q. You, C. P. Sun, and F. Nori, Controlling a nanowire spin-orbit qubit via electric-dipole spin resonance, *Phys. Rev. Lett.* **111**, 086805 (2013).
- [30] M. P. Nowak and B. Szafran, Spin-polarization anisotropy in a narrow spin-orbit-coupled nanowire quantum dot, *Phys. Rev. B* **87**, 205436 (2013).
- [31] J. Romhányi, G. Burkard, and A. Pályi, Subharmonic transitions and bloch-siegert shift in electrically driven spin resonance, *Phys. Rev. B* **92**, 054422 (2015).
- [32] D. Khomitsky, E. Lavrakhina, and E. Sherman, Spin rotation by resonant electric field in few-level quantum dots: Floquet dynamics and tunneling, *Phys. Rev. Applied* **14**, 014090 (2020).
- [33] R. Li, A spin dephasing mechanism mediated by the interplay between the spin-orbit coupling and the asymmetrical confining potential in a semiconductor quantum dot, *Journal of Physics: Condensed Matter* **30**, 395304 (2018).
- [34] D. V. Khomitsky, E. A. Lavrakhina, and E. Y. Sherman, Electric dipole spin resonance at shallow donors in quantum wires, *Phys. Rev. B* **99**, 014308 (2019).
- [35] R. Li, Charge noise induced spin dephasing in a nanowire double quantum dot with spin-orbit coupling, *Journal of Physics: Condensed Matter* **32**, 025305 (2020).
- [36] Y. Li, L. P. Pitaevskii, and S. Stringari, Quantum tricriticality and phase transitions in spin-orbit coupled bose-einstein condensates, *Phys. Rev. Lett.* **108**, 225301 (2012).
- [37] Y. Li, G. I. Martone, L. P. Pitaevskii, and S. Stringari, Superstripes and the excitation spectrum of a spin-orbit-coupled bose-einstein condensate, *Phys. Rev. Lett.* **110**, 235302 (2013).
- [38] Y. Ban, X. Chen, J. G. Muga, and E. Y. Sherman, Quantum state engineering of spin-orbit-coupled ultracold atoms in a morse potential, *Phys. Rev. A* **91**, 023604 (2015).
- [39] R. M. Lutchyn, J. D. Sau, and S. Das Sarma, Majorana fermions and a topological phase transition in semiconductor-superconductor heterostructures, *Phys. Rev. Lett.* **105**, 077001 (2010).
- [40] Y. Oreg, G. Refael, and F. von Oppen, Helical liquids and majorana bound states in quantum wires, *Phys. Rev. Lett.* **105**, 177002 (2010).
- [41] M. Wu, J. Jiang, and M. Weng, Spin dynamics in semiconductors, *Physics Reports* **493**, 61 (2010).
- [42] D. Csontos, P. Brusheim, U. Zülicke, and H. Q. Xu, Spin- $\frac{3}{2}$ physics of semiconductor hole nanowires: Valence-band mixing and tunable interplay between bulk-material and orbital bound-state spin splittings, *Phys. Rev. B* **79**, 155323 (2009).
- [43] D. Csontos, U. Zülicke, P. Brusheim, and H. Q. Xu, Landé-like formula for the g factors of hole-nanowire subband edges, *Phys. Rev. B* **78**, 033307 (2008).
- [44] P. Lawaetz, Valence-band parameters in cubic semiconductors, *Phys. Rev. B* **4**, 3460 (1971).
- [45] M. Sweeny, J. Xu, and M. Shur, Hole subbands in one-dimensional quantum well wires, *Superlattices and Microstructures* **4**, 623 (1988).
- [46] P. C. Sercel and K. J. Vahala, Analytical formalism for determining quantum-wire and quantum-dot band structure in the multiband envelope-function approximation, *Phys. Rev. B* **42**, 3690 (1990).
- [47] Y. A. Bychkov and E. I. Rashba, Oscillatory effects and the magnetic susceptibility of carriers in inversion layers, *Journal of Physics C: Solid State Physics* **17**, 6039 (1984).